ISSN 1024-8560, Atmospheric and Oceanic Optics, 2024, Vol. 37, No. 6, pp. 833–841. © Pleiades Publishing, Ltd., 2024.
Russian Text © The Author(s), 2024, published in Optika Atmosfery i Okeana.

REMOTE SENSING OF ATMOSPHERE, HYDROSPHERE, AND UNDERLYING SURFACE

Influence of the "Cloud Bow" Effect in SEVIRI Measurements on the Retrieval of the Diurnal Cycle of Land–Sea Cloud Liquid Water Path Contrast in Northern Europe

V. S. Kostsov[a], *, D. V. Ionov[a], A. B. Andryukova[a], and E. P. Ryabushko[a]

[a] *St. Petersburg State University, St. Petersburg, 198504 Russian Federation*

**e-mail: v.kostsov@spbu.ru*

Received March 12, 2024; revised May 21, 2024; accepted June 19, 2024

Abstract—The information on the cloud liquid water path (LWP) is required for many applications including global and regional climate modelling, weather forecasting, and hydrological cycle modelling. The results of derivation of the land–sea LWP contrast from LWP measurements with the satellite SEVIRI (Spinning Enhanced Visible Infra-Red Imager) instrument over land and water bodies in northern Europe are presented. The study of the diurnal cycle of the LWP contrast for some water bodies discovered two maxima nearly symmetrical about the noon UTC. They were observed in most cases at measurement points in the Gulf of Riga and in the Gulf of Finland in the Baltic Sea. Presumably, those maxima were artefacts of observations caused by the so-called "cloud bow effect." Calculations of a scattering angle for the satellite measurements at these points confirm this conclusion. The problems of data filtering and analyzing in the cases of manifestation of this disturbing effect are discussed. An approach to data analysis is suggested. This approach and the results can be used to assess the quality of LWP measurements by SEVIRI in various regions of the globe.

Keywords: cloud liquid water path, troposphere, inhomogeneities of atmospheric parameters, diurnal cycle of atmospheric parameters, remote sensing, meteorological satellite, SEVIRI

DOI: 10.1134/S1024856024701094

INTRODUCTION

The satellite instrument SEVIRI (Spinning Enhanced Visible Infra-Red Imager) measures cloud parameters with high spatial and temporal resolution, thus enabling studying cloudiness properties on the global scale. SEVIRI is a 12-channel scanning radiometer which operates in the visible and infrared spectral regions. It is mounted onboard *Meteosat* geostationary meteorological satellites and scans a large area of the Earth's surface, which is designated by a special term "SEVIRI disk" [1]. The main orbital position of a satellite is above the equator near zero longitude, which makes possible measurements over Europe, Africa, the Atlantic, part of South America, and part of the Indian Ocean. The spatial resolution at a subsatellite point is 3 km. The scanning frequency provides receiving data once every 15 min over any surface point. The SEVIRI products are atmospheric and cloud parameters, which are retrieved with a complex algorithm using so-called "lookup tables." These tables are preliminarily calculated for a set of atmospheric states and underlying surface parameters. The detailed description of the algorithm, the radiative transfer models used, and the block diagram of the algorithm can be found in [2].

The cloud liquid water path (LWP), which shows the total mass of the liquid water droplets in a column of a unit cross section, is one of the most important cloud characteristics. It is used in solutions of different problems of weather forecasting and climatology. Data on the LWP are among products retrieved from SEVIRI measurements. The detailed analysis of the statistical characteristics of the LWP for different cloud types derived from SEVIRI measurements can be found, for example, in work [3]. That work showed each cloud type to be characterized by a certain LWP distribution function constant in time throughout the Earth's surface area scanned by SEVIRI. However, detailed examination of individual regions, such as Central Europe, revealed significant variations in the LWP. The study of relative diurnal variations in the LWP showed them to be most pronounced for lower and middle-level clouds. It was also noted that the mean LWP is higher over land than over sea; according to measurements of 2009, this difference was 15–27% for low-level clouds.

In [4], we analyzed the difference in the LWP over land and sea in northern Europe based on SEVIRI measurements. Hereinafter, we use the term "land–sea LWP contrast," which we define as the difference

between LWP values over land near a water body (sea, bay, or lake) and over this water body. The analysis of the statistical distributions of the LWP contrast and its intraseasonal variations enabled us to reveal several effects which we classified as manifestations of errors in the algorithm of processing raw SEVIRI data (measurements of reflected solar radiation), including a sharp and simultaneous decrease in the LWP contrast in the early August each year at different measurement points in the Gulf of Finland and the Gulf of Riga and a complete absence of negative values of the LWP contrast in the statistical distributions for certain measurement points.

In this work, we continue study [4], but with the diurnal cycle of the land–sea LWP contrast as the main object. The aims of the work are to identify regularities in this diurnal cycle and to detect possible artefacts similar to those described in detail in [4].

INITIAL DATA

Initial data in this work are SEVIRI information products, processing version No. 2, retrieved from measurements in 2011–2017 [5]. The geographic region under study is ~700 × 700 km in size, with the center at St. Petersburg, Russia. The horizontal size of a ground pixel in SEVIRI measurements is ~7 km for this region of the Earth's surface. The input data set included the LWP only for liquid droplet clouds; data for ice and mixed clouds were filtered out during the initial stage. It is important to note that the initial data set includes measurements both under cloudy and clear-sky conditions, since the focus of our study is not LWP values, but their difference (contrast), which is obviously the most pronounced when there are clouds over one point and the sky is clear over another.

It is important to emphasize that we consider not the full daily cycle of the LWP contrast, but only its variation in the daytime, since SEVIRI measurements are based on reflected solar radiation, i.e., during daylight hours. It should be noted that the data corresponding to a solar zenith angle more than 72° were filtered out, since the errors in these data were maximal. This rejection of SEVIRI data is standard [2, 6].

The LWP contrast is analyzed for several pairs of points above large water bodies and land near them, but not throughout the region. We tried to select points above land and water so as the line connecting them was oriented close to the south–north direction to avoid the influence of cold air transfer from water bodies to land by westerly winds prevailing (along with southwesterly winds) in the region of the Gulf of Finland. Below, a pair of points is referred to as one "contrast measurement point." These measurement points are shown in Fig. 1, which is adopted from [4]. In this paper, we preserved the original designations (ML – measurement location, followed by the point number). The rationale for choosing the measurement points, the exact coordinates, and other information can be found in [4]. The largest number of points was selected in the Gulf of Finland, since artefacts in the LWP contrast values were revealed for that water body.

RESULTS

Diurnal Cycle of LWP Contrast

We describe the diurnal cycle of the land–sea LWP contrast in terms of mean values each related to a specific time point of SEVIRI measurements (with a frequency of one measurement every 15 min). During the first stage, the averaging was performed over seven years of observations. Due to the short period of solar illumination in the cold season, we selected only summer for the analysis and separately studied each month. In this paper, we did not consider August data, since our work [4] discovered the so-called "August anomaly" characterized by near zero LWP contrast, which was assumed to be an artefact of measurements.

Figure 2 shows typical examples of the averaged diurnal variations in the land–sea LWP contrast at two measurement points in the Gulf of Riga and Gulf of Finland of the Baltic Sea in June and July. One can see two most significant local maxima symmetrical about the noon UTC, near 11:00 and 16:00 of local time. The vertical bars show the standard errors of the mean values at each time point (the standard deviation of a sample divided by the square root of the sample size). These bars are relatively large because of the high variability of LWP contrast and the limited amount of data for averaging. We emphasize that the number of available initial measurements for one mean value varied from several dozens to 100 or more. As a result, oscillations are sometimes noticeable in the figures.

As can be seen in Fig. 2, the local maxima (*1* and *2*) are significant; they much exceed the standard errors in the means if the contrast values one hour before and one hour after a maximum are taken as basic. It is important that these features of the diurnal cycle observed at the same time at different geographical points can be explained neither by random measurement noise nor by physical mechanisms of cloud formation processes.

Table 1 provides complete information on the presence/absence of the first and second local maxima in the diurnal cycle of the LWP contrast at all measurement points similar to those shown in Fig. 2. When analyzing the data, the statistical significance of the maxima was assessed by the parameter

$$A(t) = \frac{D_2 - \left((D_1 + D_3)/2\right)}{\sigma_A}, \qquad (1)$$

where t is the time of recording the first or second local maxima; D_i are the LWP contrast means over three consecutive equal time spans Δt_i with the second span centered at time t; σ_A is the standard error in A calculated from the errors in D_i. The physical basis of that

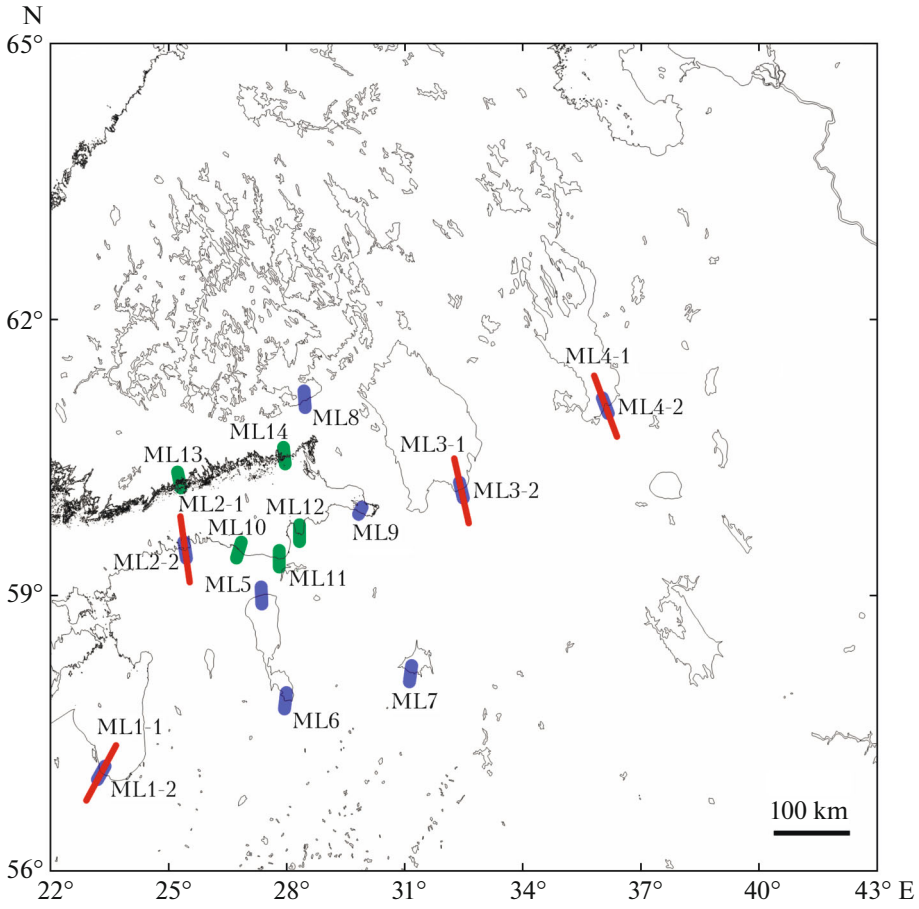

Fig. 1. The geographic region and specific points selected for the study of LWP contrast. Points ML1–ML14 (see text) are shown as lines connecting ground-based SEVIRI measurement pixels over land and water: long thin lines (ML1-1, ML2-1, ML3-1, and ML4-1) show the LWP contrast at a large distance (about 80 km), short heavy lines (ML1-2, ML2-2, ML3-2, and ML4-2) show the LWP contrast at small distances (about 20 km); ML10–ML14 are "additional" measurement points in the Gulf of Finland. The figure is adopted from [4].

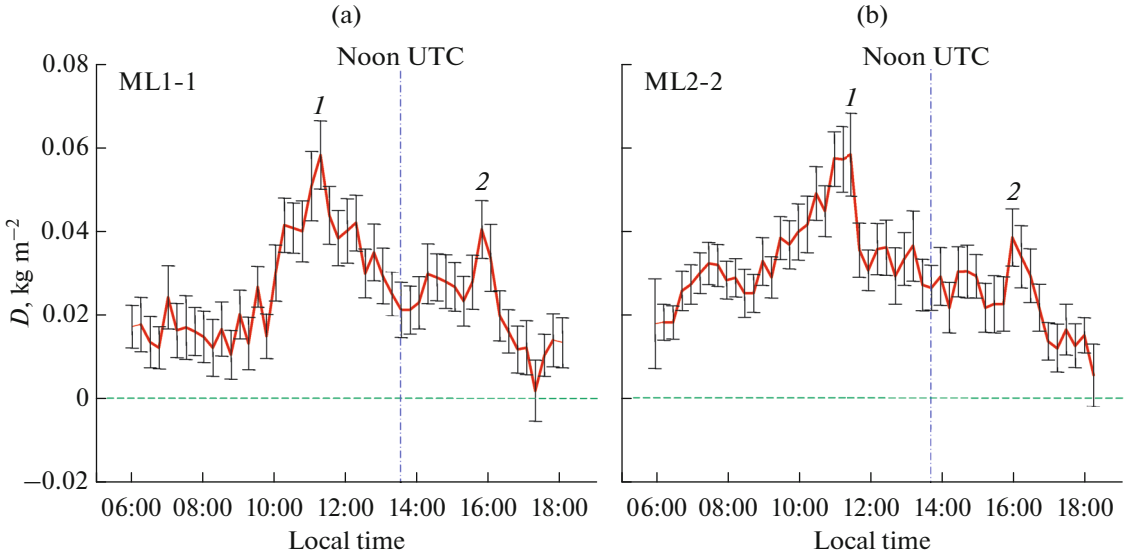

Fig. 2. Seven-year (2011–2017) average diurnal cycles of the land–sea LWP contrast D (solid curves) at a measurement point (a) in the Gulf of Riga in June and (b) in the Gulf of Finland in July: two local maxima symmetrical about the noon UTC (*1* and *2*); zero LWP contrast (horizontal dashed line); standard errors of LWP contrast means (bars).

Table 1. The presence of the 1st and 2nd local maxima (about 11:00 and 16:00 of local time) in the daily cycle of the LWP contrast at main chosen measurement points (0 means the absence of maximum and 1 means the presence of a maximum): averaging over 2011–2017

Water area	Measurement point	The presence of local maximum in the diurnal variation in the LWP contrast (A)	
		June	July
1. Gulf of Riga	ML1-1	1 (3.0)/1 (2.4)	1 (3.7)/1 (3.3)
	ML1-2	1 (2.5)/1 (3.3)	1 (3.0)/1 (2.1)
2. Gulf of Finland	ML2-1	0 (0.2)/1 (2.1)	1 (3.7)/0 (1.2)
	ML2-2	0 (1.8)/1 (2.7)	1 (3.0)/1 (2.5)
3. Lake Ladoga	ML3-1	0 (0.6)/1 (2.7)	0 (1.7)/0 (0.2)
	ML3-2	0 (0.8)/0 (1.0)	0 (0.4)/0 (0.1)
4. Lake Onega	ML4-1	0 (1.9)/0 (1.3)	0 (0.2)/0 (0.2)
	ML4-2	0 (1.3)/0 (0.3)	0 (1.8)/0 (1.3)
5. Lake Peipus	ML5	0 (0.5)/0 (0.3)	1 (2.4)/0 (1.4)
6. Lake Pihkva	ML6	0 (0.2)/0 (0.3)	0 (1.0)/0 (0.2)
7. Lake Ilmen	ML7	0 (0.2)/0 (0.8)	0 (0.3)/0 (1.0)
8. Saimaa	ML8	0 (1.0)/0 (0.8)	0 (1.2)/0 (1.7)
9. Neva Bay	ML9	1 (3.1)/0 (0.1)	1 (3.6)/0 (0.9)
10. Gulf of Finland, Kalvi	ML10	1 (3.0)/1 (2.2)	1 (2.9)/0 (1.8)
11. Narva Bay	ML11	0 (1.5)/0 (0.7)	0 (1.5)/0 (1.6)
12. Luga Bay	ML12	1 (2.7)/0 (1.3)	1 (4.2)/0 (1.2)
13. Gulf of Finland, Helsinki	ML13	1 (2.9)/1 (2.9)	0 (1.6)/1 (2.2)
14. Gulf of Finland, Torfyanovka	ML14	1 (2.6)/0 (1.3)	1 (3.6)/0 (0.5)

criterion was the a priori assumption that time intervals of the appearance of local maxima are known and sufficiently short. Calculations were carried out for two time points $t_1 = 11.3$ h and $t_2 = 16$ h at $\Delta t_i = 1$ h. Parameter A characterizes the magnitude of the excess of the LWP contrast means during the period of possible appearance of a local maximum over the means before and after this event. A local maximum can obviously be considered statistically significant if $A(t) > 2$.

It is easy to see these local maxima in the average diurnal cycle of the LWP contrast at all points in the Baltic Sea except for point ML-11 located in the Narva Bay. Note also that local maxima are absent for all lakes except for Ladoga and Peipus, where the second maximum is manifested in June and the first maximum is pronounced in July. These results point out either to physical processes which run in the Baltic Sea and induce the appearance of short-term LWP contrast maxima at the same local astronomical time points at all measurement points or to the artefact of measurements. Two circumstances support the second hypothesis. First, the maxima are always observed symmetrically about noon UTC; hence, they are most likely connected to the measurement geometry determined by satellite and Sun positions and are hardly caused by local physical processes. Second, artefacts in the SEVIRI data were discovered in [4] precisely when analyzing measurements in the Baltic Sea region.

Cloud Bow Effect in SEVIRI Measurements

SEVIRI records reflected solar radiation. Here, a brief explanation of the terminology used in this article is required. When considering the macroscale system, i.e., the system which includes the Sun, the Earth with its atmosphere as a single "disk" formed by the common field of view of the instrument, and a satellite carrying SEVIRI, it is convenient to use the term "reflection" to describe the transfer of solar radiation in the general measurement geometry. If we consider a microscale system, i.e., an elementary volume where solar radiation is scattered by an ensemble of cloud droplets and the scattering is characterized by the scattering phase function, it is more correct to use the term "scattering" and talk about a scattering angle.

For the measurement type under study, different atmospheric optical effects are possible which can result in "interfering" signals. The most known effect is the so-called sun glint, which appears during the

specular reflection of solar radiation from the underlying surface. The "glory" effect can appear at scattering angles near 180°. At certain scattering angles significantly lower than 180° the so-called "cloud bow effect" can be observed, caused by the refraction and reflection of rays in cloud droplets. The physics of emergence of these and other known atmospheric effects and examples of their observation can be found in [7].

Work [8] specially studied the conditions for occurrence of glory and cloud bow effects in SEVIRI measurements of reflected solar radiation. That work, like our study, considered only liquid droplet clouds. Model calculations in [8] showed that the cloud bow effect manifests itself in the scattering phase function as local "peaks" at scattering angles close to 140° (deviations from 140° are caused by variations in the characteristic size of cloud droplets). If these peculiarities of solar radiation transfer are ignored (or inadequate initial information is used for considering them), then they can manifest themselves in a certain way in final information products of satellite observations.

The diurnal cycle of the scattering angle Θ for the selected points of SEVIRI measurements is calculated with the use of equation [8]:

$$\Theta = \arccos(\sin\theta_0 \sin\theta \cos\Delta\varphi - \cos\theta_0 \cos\theta), \quad (2)$$

where θ_0 is the solar zenith angle; θ is the angle of the direction to a satellite;

$$\Delta\varphi = 180° - |\varphi - \varphi_0| \quad (3)$$

is the relative azimuth angle between the directions to the satellite and the Sun.

Figure 3 exemplifies the diurnal cycle of the solar radiation scattering angle during observations at point ML1-1 (Gulf of Riga) on June 15, 2014, and July 15, 2017. The figure contains several curves each corresponding to one of the *Meteosat* geostationary satellites operated at those time points. The longitudes of the subsatellite points for *Meteosat-8*, *9*, and *10* satellites (Fig. 3a) are 3.48; 9.31, and 0.51°, respectively, and for *Meteosat-8*, *9*, *10*, and *11* satellites (Fig. 3b) are 41.62; 9.39; –0.17, and –3.64°, respectively (positive values are eastern and negative values are western longitude). Orbital data for currently operating *Meteosat* satellites and archived orbital data are available on website https://user.eumetsat.int/resources/service-statuses/meteosat-orbital-parameters.

As noted in Introduction, the main satellite position for measurements is above the equator near the prime meridian. It is evident from Fig. 3 that several satellites can be located near this position at the same time. One of them is the main, and the others are reserve. The satellite status (main/reserve), as well as the orbit parameters, in particular subsatellite point longitude, can change with time. The arrays of LWP measurements at our disposal do not include information about a specific satellite and its orbit parameters at the time of measurements. Therefore, we can proceed from the spread of the longitudes of subsatellite points of active satellites when estimating the probability of the cloud bow effect. This spread indicates that cloud bow effect is manifesting itself for approximately one hour twice a day symmetrically about noon UTC. The interval between these events is from 3.5 to 4 h.

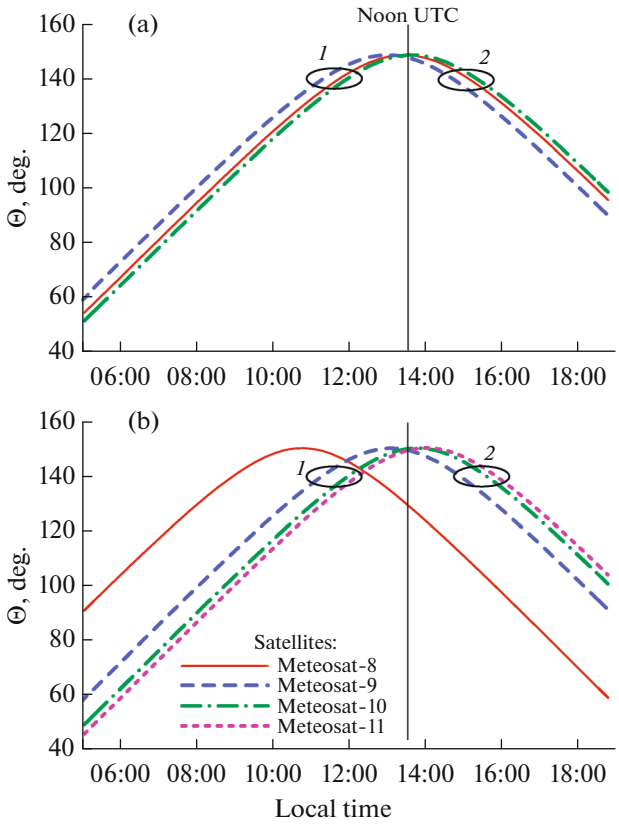

Fig. 3. Diurnal cycle (local astronomical time) of the solar radiation scattering angle for ML1-1 measurement point in the Gulf of Riga of the Baltic Sea on (a) June 15, 2014, and (b) July 15, 2017, for several active *Meteosat* satellites (see legend). Ovals with numbers *1* and *2* show areas of probable manifestation of the cloud bow effect when the scattering angle is close to 140°.

Note that the time interval between the local LWP contrast maxima in Fig. 2 is ~4.5 h. If we assume that the cloud bow effect takes place at an angle of <140°, for example, 136°, then, as can be seen from Fig. 3, the interval between the manifestations of this effect is 4.5 h. The range of scattering angles where the cloud bow effect is possible is 135°–140° [9]. The symmetry about noon UTC is explained by the fact that the subsatellite point of the main measuring satellite is close to the prime meridian. If, for example, *Meteosat-11* was the main satellite on July 15, 2017, located at 41° east of the prime meridian, then the effects would be observed symmetrically about noon at the longitude of

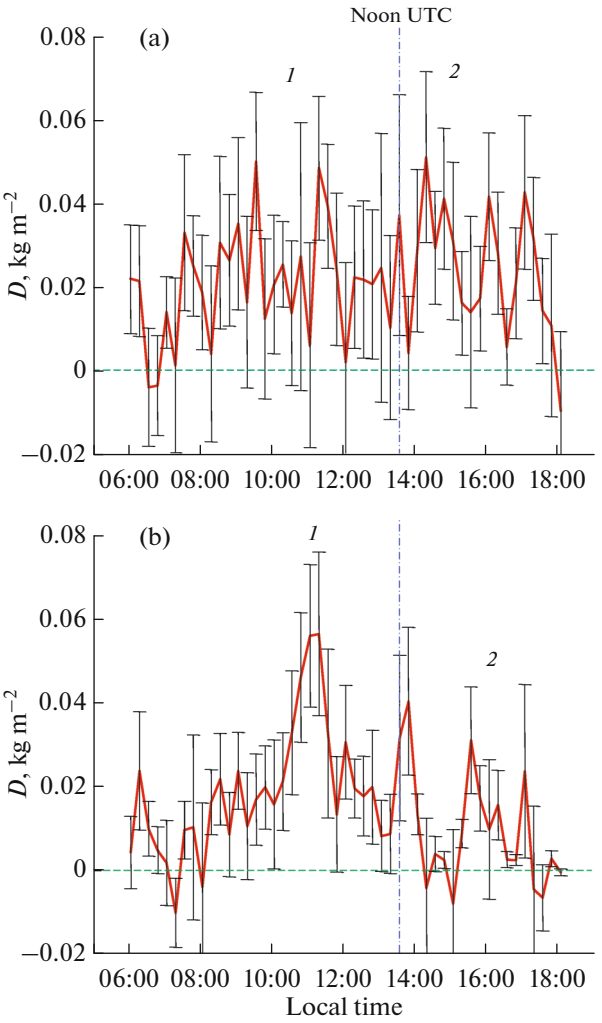

Fig. 4. Average diurnal cycles of the land–sea LWP contrast D (solid curves) for ML1-1 measurement point in the Gulf of Riga in (a) June 2012 and (b) June 2016: time points of two typical local maxima caused by the cloud bow effect (*1* and *2*); other designations see in Fig. 2.

that satellite. We emphasize that we are talking about geostationary satellites in this work.

Thus, the observed local LWP contrast maxima are, with a very high degree of probability, caused by the cloud bow effect at scattering angles close to 140°.

Rejection of Erroneous Measurements and the Analysis of Diurnal Cycle with False Maxima

Rejection of erroneous measurements which contain the unaccounted signal component caused by the cloud bow effect is a difficult task due to a number of reasons. The main one is the unpredictability of the manifestation of this effect. The proximity of Θ to 140° is a necessary but not sufficient condition for the effect to be manifested in measurements. Note that we are talking just about the manifestation of the effect in information products, since a local peak is always present in the scattering phase function at $\Theta = 140°$, and the magnitude and shape of the peak are determined by the effective radius and width of the cloud droplet size distribution [8]. It should be remembered that there is uncertainty in calculations of the scattering angle if information about the longitude of the subsatellite point of a main satellite, i.e., the satellite which carries the instrument which measures at that time, is absent for each specific measurement. As the above examples show, the longitude can vary within 10°, which leads to uncertainty in the time of manifestation of the cloud bow effect of about an hour. The presence of liquid droplet clouds is obviously the additional mandatory condition for the manifestation of the effect. In this case, an interfering signal caused by the cloud bow effect should exceed the variations in the useful signal caused by the natural short-term changes in the atmospheric parameters and clouds.

Cloudiness is so strongly variable in space and time that the problem of detecting the cloud bow effect in measurements on a specific day at a specific time points against the background of natural variations can be considered unsolvable. It is easy to imagine a situation where clouds are much thicker before and after the time when Θ is close to 140° than at the time of appearance of a "cloud bow." In this case, the effect is unnoticeable and, with a high degree of probability, the variation in the measured signal can be attributed to the natural variability of the cloudiness parameters. This implies an important conclusion: the cloud bow effect can be detected only in measurements made at a scattering angle close to 140° and averaged over a long period (e.g., several years), like in our case. For illustration, Fig. 4 shows average diurnal variations in the LWP contrast in June 2012 and 2016 at the ML1-1 measurement point. There are no signs of the presence of the cloud bow effect around 11:00 and 16:00 of local astronomical time in June 2012. About 10 approximately identical local LWP contrast maxima are seen during a day, which are most likely due to variations in cloud parameters. The second example (June 2016) shows a rare case where a local LWP contrast maximum (the first one) stands out against the other local maxima even when averaging over one month of only one year, and it is impossible to distinguish the second local maximum against several other nearby local maxima.

Another important remark should be made about the manifestation of the cloud bow effect in SEVIRI information products. According to [8], the processing algorithm for measurements of scattered solar radiation basically takes into account the cloud bow effect, since scattering phase functions which describe this effect are used in calculating lookup tables. An artefact appears in the results when the initial information on cloud droplet size distribution does not correspond to the actual cloud situation during the measurements. The error spreads throughout the algo-

rithm and manifests itself in the results. Therefore, it is impossible to predict the sign and magnitude of the artefact.

Since it is impossible to detect single measurements which contain an interfering component caused by the cloud bow effect, we should analyze the results which contain this component. As can be seen from the presented diurnal cycles and the calculations of the scattering angle during measurements, the cloud bow effect is manifesting itself during two relatively short periods of time of no longer than an hour. Therefore, using an approximation for smoothing the initial function, it is possible to minimize the disturbance of the diurnal cycle due to this effect. Since the diurnal cycle is strongly determined by convective processes induced by surface heating by solar radiation, we can reliably consider these processes to be significantly slower compared to the cloud bow effect in measurements with high degree of confidence. Using a smooth approximation, we not only reduce the cloud bow effect, but also eliminate oscillations due to random measurement errors of various kinds.

Figure 5 shows the results of approximation of the monthly average diurnal variation in the LWP contrast by a 7th-degree polynomial. The results were obtained through averaging the data over all seven years of observations. The approximation was performed both for the complete data sets and for the sets where potentially erroneous observations were rejected, i.e., all observations during two short (no more than an hour) periods of time when the cloud bow effect could manifest itself. The 7th-degree polynomial was chosen as providing the maximal determination coefficient and the minimal standard deviation in the absence of "false" local short-term features in the diurnal variation. The determination coefficient is within the range 0.70–0.88 for all the measurement points when approximating by the 7th-degree polynomial. The standard deviation of the approximated values from experimental ones is within the range 0.005–0.006 kg m^{-2}.

The main conclusion which can be drawn from the results presented in Fig. 5 is that the smooth approximation curves derived for the data with and without rejection show the same diurnal cycle for all the considered geographical points. The systematic overestimation of the contrast by the approximation curve can be considered insignificant even during the periods of pronounced manifestation of the cloud bow effect (points ML1-1, ML2-2, and ML13). If the effect is not manifested (point ML11) or one of the local maxima is not expressed (point ML9, the second maximum) (see Table 1), then the approximation curves for the data with and without rejection near coincide.

Figure 5 enables quite accurate estimation of the features of the daily cycle of the LWP contrast for the Gulf of Finland and the Gulf of Riga of the Baltic Sea in June and July: an increase in the LWP contrast from 06:00 to 07:00, stabilization for one hour, a further increase until 11:00, then a decrease until 14:00–15:00, relative constancy until 16:00–17:00, and again a decrease.

DISCUSSION

The statistics and causes of erroneous measurements of reflected solar radiation from space platforms was studied in detail in [9] for the MODIS satellite instrument. The MODIS and SEVIRI instruments have the same measurement principle and similar algorithms for processing results based on precalculated lookup tables.

The causes of erroneous measurements are numerous. Here, we list only some of them: nonuniformity of cloudiness on subpixel scales, optical effects (sun glint, glory, and cloud bow), overlapping of cloud layers, incorrect identification of the phase of cloud particles, rain clouds, drizzling clouds, incorrect assessment of the degree of discontinuity of cloud cover during observations at large angles (this effect is significant for measurement points at the edge of a measurement area, the so-called disk), 3D effects at large observation angles in the presence of deep towering clouds. The cloud bow effect on the general statistics of satellite measurements of reflected solar radiation cannot be called negligible: for example, work [9] shows this effect to cause the rejection of 25% of pixels in MODIS measurements in the presence of marine single-level liquid droplet clouds in the field of view of the instrument.

The fact that the cloud bow effect was detected in June and July only for the measurement points in the bays of the Baltic Sea and was not detected at measurement points near large and small lakes is important. Since the previous work [4] detected artefacts in SEVIRI measurements just in the bays of the Baltic Sea, we can conclude with a high degree of probability that we also deal with an artefact in the case under study, which is apparently caused by the specifics of using the processing algorithm for initial measurements of reflected solar radiation in the Baltic Sea region. A list of the so-called algorithmic causes of erroneous measurements can be found in [9]: coding errors, methodological errors in the selection of parameters and threshold values of different criteria, and the use of inappropriate additional information. The study of these causes is beyond the scope of our work.

CONCLUSIONS

In this work, we have focused on the manifestation of the cloud bow effect in the results of retrieving the land–sea LWP contrast from SEVIRI measurements of LWP over land and water bodies in northern Europe. Two maxima have been found in the diurnal cycle of the LWP contrast for some water bodies; they

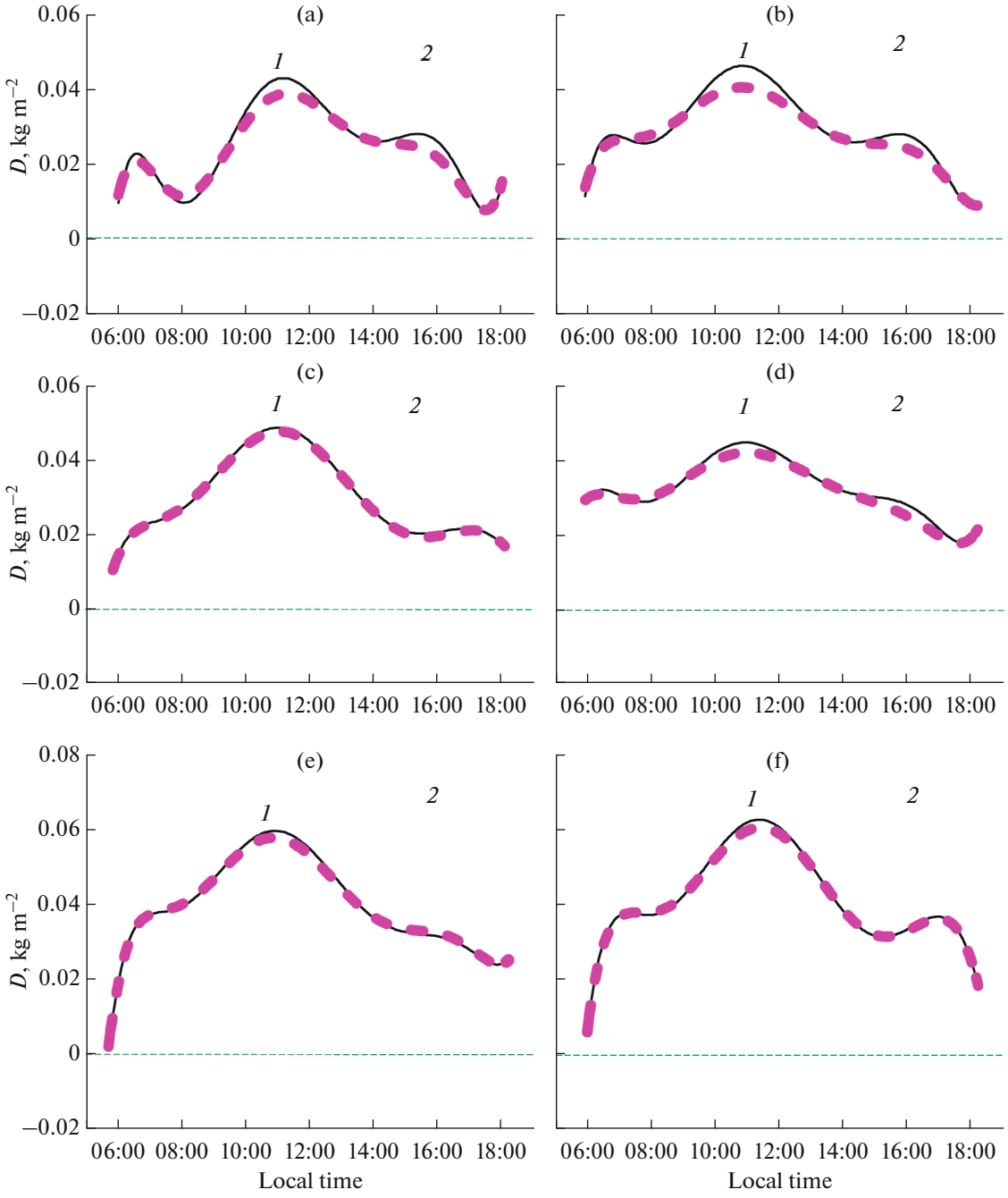

Fig. 5. Approximation by 7th-degree polynomials of the seven-year (2011–2017) average diurnal cycles of the land–sea LWP contrast for several measurement points in the bays of the Baltic Sea: (a) ML1-1, June; (b) ML2-2, July; (c) ML11, June; (d) ML13, July; (e) ML9, June; (f) ML9, July, without (solid curve) and with (dashed curve) rejection of potentially erroneous data during the periods of the cloud bow effect. The time points of manifestation of the effect (11:00 and 16:00) are shown by figures *1* and *2*; the horizontal dashed line corresponds to zero LWP contrast.

are almost symmetrical about noon UTC. In most cases, these maxima are observed in measurements at points in the Riga and Finland Gulfs of the Baltic Sea, and are not observed in the regions of small and large lakes (Ladoga, Onega, Peipus, Pihkva, Ilmen, and Saimaa). The calculations of the solar radiation scattering angle for measurements at these points have shown the local maxima to coincide with the periods when the cloud bow effect is possible, i.e., at a scattering angle of 135°–140°. Thus, these maxima are probably artefacts of observations caused by this effect.

Due to the significant spatiotemporal variability of cloudiness, it is impossible to identify and reject individual SEVIRI measurements which contain an inter-

fering component caused by the cloud bow effect. The calculations have shown that approximation of the diurnal cycle by a 7th-degree polynomial enables reducing the effect of the interfering component and tracking the main features of the diurnal cycle. The use of the approximation enables us to completely reject all measurements corresponding to scattering angles of 135°–140° in advance; however, even without this rejection, the error caused by the presence of erroneous results is negligibly small and amounts to 0.001–0.006 kg m^{-2} (2–14%) in the cases under study. After polynomial approximation of the diurnal cycle of the LWP contrast, the following features were discovered for the Gulf of Finland and Gulf of Riga of the Baltic Sea in June and July: an increase in the LWP contrast from 06:00 to 07:00, stabilization for an hour, a further increase until 11:00, then a decrease until 14:00–15:00, a relative constancy of values until 16:00–17:00, and a decrease again.

FUNDING

The work was supported by the Russian Science Foundation (grant no. 24-27-00016, https://rscf.ru/project/24-27-00016/).

CONFLICT OF INTEREST

The authors of this work declare that they have no conflicts of interest.

REFERENCES

1. J. Schmetz, P. Pili, S. Tjemkes, D. Just, J. Kerkmann, S. Rota, and A. Ratier, "An introduction to Meteosat Second Generation (MSG)," Bull. Am. Meteorol. Soc. **83**, 977–992 (2002). https://doi.org/10.1175/1520-0477(2002)083<0977:AITMSG>2.3.CO;2
2. R. A. Roebeling, A. J. Feijt, and P. Stammes, "Cloud property retrievals for climate monitoring: Implications of differences between Spinning Enhanced Visible and Infrared Imager (SEVIRI) on METEOSAT-8 and Advanced Very High Resolution Radiometer (AVHRR) on NOAA-17," J. Geophys. Res. **111**, 20210 (2006). https://doi.org/10.1029/2005JD006990
3. A. Kniffka, M. Stengel, M. Lockhoff, R. Bennartz, and R. Hollmann, "Characteristics of cloud liquid water path from SEVIRI onboard the Meteosat Second Generation 2 Satellite for several cloud types," Atmos. Meas. Tech. **7**, 887–905 (2014). https://doi.org/10.5194/amt-7-887-2014
4. V. S. Kostsov and D. V. Ionov, "Specific features of the land-sea contrast of cloud liquid water path in Northern Europe as obtained from the observations by the SEVIRI instrument: Artefacts or reality?," Meteorology **2** (4), 464–488 (2023). https://doi.org/10.3390/meteorology2040027
5. N. Benas, S. Finkensieper, M. Stengel, G.-J. van Zadelhoff, T. Hanschmann, R. Hollmann, and J. F. Meirink, "The MSG-SEVIRI-based cloud property data record CLAAS-2," Earth Syst. Sci. Data **9**, 415–434 (2017). https://doi.org/10.5194/essd-9-415-2017
6. M. Kim, J. Cermak, H. Andersen, J. Fuchs, and R. A. Stirnberg, "New satellite-based retrieval of low-cloud liquid-water path using machine learning and Meteosat SEVIRI data," Remote Sens. **12**, 3475 (2020). https://doi.org/10.3390/rs12213475
7. G. P. Konnen, "Rainbows, halos, coronas and glories. Beautiful sources of information," Bull. Am. Meteorol. Soc. **98**, 485–494 (2017). https://doi.org/10.1175/ BAMS-D-16-0014.1
8. N. Benas, J. F. Meirink, M. Stengel, and P. Stammes, "Sensitivity of liquid cloud optical thickness and effective radius retrievals to cloud bow and glory conditions using two SEVIRI imagers," Atmos. Meas. Tech. **12**, 2863–2879 (2019). https://doi.org/10.5194/amt-12-2863-2019
9. H.-M. Cho, Z. Zhang, K. Meyer, M. Lebsock, S. Platnick, A. S. Ackerman, L. Di. Girolamo, L. C. Labonnote, C. Cornet, J. Riedi, and R. E. Holz, "Frequency and causes of failed MODIS cloud property retrievals for liquid phase clouds over global oceans," J. Geophys. Res.: Atmos. **120**, 4132–4154 (2015). https://doi.org/10.1002/2015JD023161

Translated by O. Ponomareva